

Non-Markovian Dynamics in Fiber Delay-Line Buffers

Kim Fook Lee and Prem Kumar¹

¹*Center for Photonic Communication and Computing,
Department of Electrical Engineering and Computer Science,
Northwestern University, 2145 Sheridan Road, Evanston, IL 60208-3112, USA**

(Dated: February 2, 2024)

Abstract

We study the non-Markovian effect on a two-photon polarization entangled state in which one photon from the pair is stored in a fiber delay-line buffer. We propose a model of a photonic qubit coupled to fiber birefringence and a fiber reservoir representing the environment. We analytically derive a non-Markovian probability function for the buffered photon and its paired photon. To verify the probability function, we perform the full quantum state tomography of the photon pairs. We further exploit the measures of quantum mutual information for studying the quantumness of the buffered photon and its paired photon. We find that Werner's well-known separability criterion occurs at the buffer time of about 0.9 ms. Furthermore, our result implies that the non-zero quantum discord can surpass Werner's criterion, and hence the quantum bi-partite correlation can exist for a buffer time greater than 0.9 ms.

INTRODUCTION

Photons that traverse in optical fiber with little attenuation are ideal carriers for quantum networking. The photonic qubits with entanglement in polarization, time-bin, or other degrees of freedom are the resources for establishing quantum communication and distributed quantum computing. Fiber-based quantum networks can provide secure internet over long distances with the help of quantum optical memories [1–4]. However, quantum memories with long storage times that utilize light-matter interactions are limited by optical bandwidth and low storage and retrieval efficiency [3, 5]. Quantum buffers made of optical fiber and free-space optics can provide a reasonable storage time (up to μsec) of the quantum states of light in different modes (polarization, time, and frequency) without significant deterioration of storage efficiency [6–13]. These buffers can be integrated with low-loss (< 1 dB) ultra-fast optical switches [14, 15] to provide multiple synchronized qubits suitable for large-scale quantum networking.

Quantum buffers based on fiber delay lines are traveling buffers[16] and fiber loop buffers [17]. The former can allocate a fixed delay. The combination of a few fixed delay lines and low-rate 2×2 switches can provide active temporal source multiplexing for high-efficiency single photon generation [11, 18, 19]. However, long storage times play an important role in optical networks for packet synchronization, label processing, and contention management. The traveling buffers, which can provide qubit storage time up to μsec , is relatively unexplored. In general, there is a strong coupling between qubits and fiber birefringence in a fiber reservoir, so we need to develop a non-Markovian model to study the decoherence dynamics of qubits in the fiber-based quantum buffer.

Recent studies [20–22] indicate that Markovian and non-Markovian processes can be controlled to improve the quantum capacity in a high-loss communication channel and model quantum networks. A comprehensive discussion of concepts, measures, and witness of non-Markovian effect for an open quantum system can be found in ref[23]. A trace distance of two quantum states is usually used to detect the crossover between the Markovian and non-Markovian process such as the coupling between the photon polarization and its optical frequency degree of freedom in a simple titled Fabry-Perot cavity platform [24]. The fiber-based quantum buffer is an open quantum system because the polarization degree of freedom of photon is coupled with the frequency degree of freedom of the fiber birefringence which

is coupled with the fiber reservoir. The non-Markovian effect can revive entanglement after observation of entanglement sudden death [25, 26].

An exactly solvable master equation of an open quantum system, such as a two-level atom interacting resonantly in a reservoir formed by the Lorentzian quantized modes of a high Q cavity, is often used as an example for illustrating the non-Markovian dynamics of a qubit [27–31]. Furthermore, the non-Markovian dynamics have been studied by using quantum discord [32, 33], which is another concept of quantum correlation introduced by quantum mutual information theory. Some believe that quantum discord is more suitable for quantifying the quantum correlation of a bipartite system in non-Markovian environments. We recently used it to explore the quantum coherence of a two-qubit entangled state generated in green fluorescent protein [34, 35] at room temperature. One can experimentally obtain quantum discord by calculating the total correlation and classical correlation based on the density matrix elements of a quantum state.

In this paper, one photon from the polarization entangled photon pair is stored in the buffer. We use a model to study the non-Markovianity of a photonic qubit coupled to fiber birefringence of a single-mode fiber in a fiber reservoir. We analytically derive the probability function for the buffered polarization qubit and its paired photon. Quantum state tomography (QST) is then performed on the entangled photon pairs. We obtain the probability function from the reconstructed density matrix. The probability function exhibits the non-Markovianity of the buffered photon experiencing the polarization modal dispersion (PMD) and the loss in the fiber reservoir. In the experiment, we also prove the existence of the Markovian process in the scenario where we replace the buffer with a free-space attenuator.

RESULTS

Here, we consider a qubit-fiber-reservoir model consisting of a photonic qubit, a single-mode optical fiber, and a fiber reservoir representing the environment as shown in Fig.1. (see Methods for the atom-cavity-reservoir model). When a photon propagates in a long optical fiber, its polarization state and transmission rate will be degraded by the fiber birefringence and a fiber reservoir. The fiber reservoir is the medium where a polarization qubit interacts/exchanges energy with the environment. The polarization of the photon with

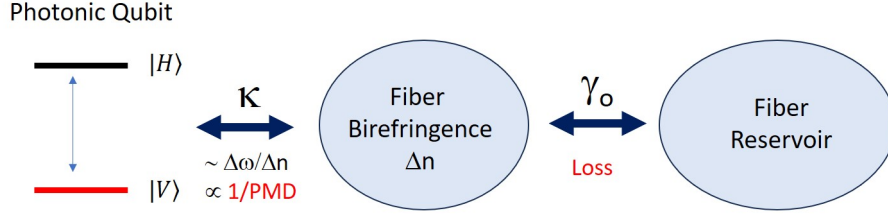


FIG. 1: A simple model consists of a photonic qubit, fiber birefringence in optical fiber, and a fiber reservoir representing the environment decoherence. The κ is the coupling constant between the qubit and fiber birefringence (Δn), so the $\kappa(\text{sec}^{-1})$ is proportional to the frequency bandwidth ($\Delta\omega$) of the qubit and inversely proportional to fiber dispersion ($dn/d\omega$). The fiber birefringence is then coupled with a fiber reservoir with the coupling constant $\gamma_o(\text{sec}^{-1})$ which is responsible for the loss of qubit information such as decoherence.

certain optical frequency bandwidth is coupled with the fiber birefringence which is coupled with the fiber reservoir. In other words, the PMD effect is coupled to the environment via the fiber reservoir. The photon polarization state will experience the dephasing caused by the PMD and the absorption/scattering process in the fiber. The absorption and re-emission of a photon state in the fiber will decohere a quantum state. A photonic qubit with polarization state H or V is coupled with the fiber birefringence by a coupling constant $\kappa \propto \frac{1}{\text{dispersion}} = 1/\frac{\Delta n}{\Delta\omega}$, where the Δn is fiber birefringence and $\Delta\omega$ is frequency bandwidth. A photonic qubit in a single optical frequency mode will couple weakly with the fiber birefringence or less dispersion (large κ), and hence experiencing less depolarization effect. If we increase the frequency bandwidth of the photonic qubit in a steep dispersion region, the κ becomes small. The qubit will start to experience the PDM effect, which is given by the square root of time variance $\langle\tau^2\rangle$ of differential group delay (DGD) [36–38] or $\sqrt{\langle\tau^2\rangle}$. Therefore, the strength of the PMD effect is inversely proportional to the κ . In other words, one can enhance the PMD effect on the photonic qubit by increasing their differential group delays such as inserting a few polarization-maintaining fiber jumpers in their channels. The same photon with optical frequency ω can be spontaneously absorbed and scattered at a rate of γ_o due to the coupling between the fiber birefringence and the reservoir. The $\gamma_o/c = \mu$ is the loss parameter per unit length of the photon due to photon absorption/scattering in the

fiber reservoir. (see Methods for the probability function of the photon state and how the relative strength of the γ_o and κ can determine the photon state undergoing Markovian and non-Markovian processes). Two factors contribute to the loss parameter. The first is the propagation loss of the photonic qubit in the fiber. The second is the loss of information on the photonic qubit which is its polarization property. The environment depolarization process can degrade the polarization extinction ratio of the qubit. The propagation loss of the photonic qubit can cause an increase in the accidental coincidence and reduce the fidelity of the quantum state. In this paper, we subtract the accidental coincidence of the signal and idler so that we can isolate the contribution of the propagation loss to the reconstructed density matrix and study the polarization property of the buffered qubit which is the idler photon.

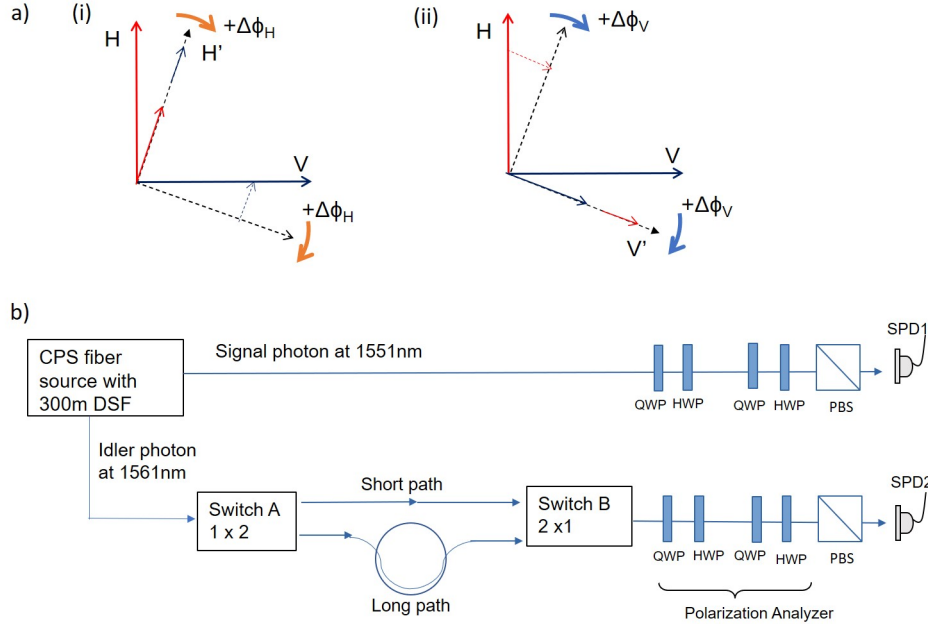


FIG. 2: a) The geometry picture for the change of polarization state (i) $H \rightarrow H'$ and (ii) $V \rightarrow V'$. Small arrows along the H' and V' showing the contribution from the H and V . The phase fluctuation $\Delta\phi$ due to PMD degrades the polarization extinction ratio of the idler. b) Experiment setup including the buffer made of two low-loss switches with a short path and a long path. We use different fiber lengths in the long path to change the buffer time.

In our two-qubit system, the photon pair is initially prepared in the entangled state

$|\psi_o\rangle = \frac{1}{\sqrt{2}}[|H_s H_i\rangle + |V_s V_i\rangle]$. One photon from the pair is sent to a buffer with the fiber length of L . Let's say the photon of interest is the idler which is experiencing the PMD and the loss in the buffer. The initial state of the idler (signal) is $|H_i\rangle + |V_i\rangle$ ($|H_s\rangle + |V_s\rangle$), respectively. Due to de-phasing caused by the PMD and fiber reservoir, the final components H_i^f and V_i^f can be written in terms of H_i and V_i as

$$\begin{aligned} H_i^f &= H_i \cos(\Delta\phi_h) + V_i \sin(\pm\Delta\phi_h) \\ V_i^f &= V_i \cos(\Delta\phi_v) - H_i \sin(\pm\Delta\phi_v) \end{aligned} \quad (1)$$

where $\pm\Delta\phi_{h(v)}$ is the amount of phase change caused by the PMD effect. The phase change $\Delta\phi_{h(v)}$ is related to the square root of time variance $\langle\tau^2\rangle$ of differential group delay (DGD) [36–38] or $\sqrt{\langle\tau^2\rangle}$. The $+$ ($-$) sign denotes the rotation of the polarization state in the clockwise (anti-clockwise) direction. The h (v) sign denotes the phase change associated with the polarization state H_i (V_i). When the $\Delta\phi_h$ and $\Delta\phi_v$ are zero, the $H_i^f \rightarrow H_i$ and $V_i^f \rightarrow V_i$. The polarization states of the idler did not change because of the absence of the PMD effect. When the $\Delta\phi_h$ and $\Delta\phi_v$ are $+90(-90)$, $H_i^f \rightarrow V_i(-V_i)$ and $V_i^f \rightarrow -H_i(+H_i)$, respectively. The polarization states of the idler are completely flipped. The geometrical meaning for these notations is shown in Fig.2a. The phase fluctuation of $\cos(\Delta\phi)$ and $\sin(\pm\Delta\phi)$ degrade the polarization extinction ratio of the idler. One can interpret that the final idler polarization state H_i^f is related to its initial states H_i and V_i at the past because of the non-Markovian effect caused by the PMD. We assume that the signal is propagating in a short fiber length before it is detected. We then obtain the probability function $\mathcal{P}_f = |\langle\psi_o|\psi^f\rangle|^2$ as,

$$\mathcal{P}_f = |\mathcal{A}[\cos(\Delta\phi_h) + \sin(\pm\Delta\phi_h) - \sin(\pm\Delta\phi_v) + \cos(\Delta\phi_v)]|^2 \quad (2)$$

where $\mathcal{A}\mathcal{A}^* = e^{-2\mu L}$ is introduced due to the loss parameter in the fiber reservoir on the polarization properties experienced by the surviving idler photons. In our experiment, we diminish the contribution of the propagation loss to the probability function by subtracting the accidental coincidence, so that we can measure the probability function which is degraded by the $\mathcal{A}\mathcal{A}^* = e^{-2\mu L}$ due to the fiber reservoir.

We explore non-Markovian dynamics of the entangled state by simplifying Eq. (2) into two cases; the magnitude of $|\Delta\phi_h| = |\Delta\phi_v|$ and $\Delta\phi_h \neq \Delta\phi_v$. For the case $\Delta\phi_h = \Delta\phi_v = \Delta\phi$,

we have the first scenario where the idler polarization states H_i^f and V_i^f rotate in opposite directions i.e we select the terms $+\Delta\phi_h$ and $-\Delta\phi_v$ or $-\Delta\phi_h$ and $+\Delta\phi_v$ in Eq. (2). The probability function \mathcal{P}_f is simplified as

$$\mathcal{P}_a \propto e^{-2\mu L} [\cos(\Delta\phi) \pm \sin(\Delta\phi)]^2 \quad (3)$$

which has a similar form as Eq. (8) in Methods for a two-level atom interacting in a high Q-cavity with a memoryless reservoir. This implies that the idler is experiencing the non-Markovian process due to the coupling between the PMD effect and the loss in the fiber reservoir. Let's consider the second scenario where the idler polarization states H_i^f and V_i^f rotate in the same directions i.e, we select the terms $+\Delta\phi_h$ and $+\Delta\phi_v$ or $-\Delta\phi_h$ and $-\Delta\phi_v$ in Eq. (2). Then the probability function \mathcal{P}_f becomes

$$\mathcal{P}_{sy} \propto e^{-2\mu L} [\cos(\Delta\phi)]^2 \quad (4)$$

which is similar to Eq. 8 for large n . We can further simplify the physical interpretation of Eq. (3) and Eq. (4) by expanding the harmonic function $\cos(\Delta\phi) = 1 - \frac{\Delta\phi^2}{2}$ and $\sin(\Delta\phi) = \Delta\phi$ with the assumption that $\Delta\phi$ is relatively small. With the substitution $\Delta\phi = \Delta\omega_i \sqrt{\langle \tau^2 \rangle} \propto L^{1/2}$ [36–38], the Eq. (3) can be approximated as $\tilde{\mathcal{P}}_a \propto e^{-2\mu L} [1 \pm \mathcal{B}L^{\frac{1}{2}} \mp \mathcal{C}L^{\frac{3}{2}} + \dots]$. The harmonic function of Eq. (3) is depending on the power of $L^{\frac{n}{2}}$, where n is the odd number. The \mathcal{B} and \mathcal{C} are the fitting parameters. On the other hand, Eq. (4) can be approximated as $\tilde{\mathcal{P}}_{sy} \propto e^{-2\mu L} [1 - \mathcal{B}'L + \mathcal{C}'L^2 + \dots]$, where the harmonic function depends on the power of L^n , n is an integer number. For the case $\Delta\phi_h \neq \Delta\phi_v$, the approximated probability function depends on the power of the fiber length $L^{\frac{n}{2}}$, where n is the positive integer number (see Methods for the complete probability function).

Later, we will verify the approximated probability function and the exact equation of Eq. (3) and Eq. (4) by launching one photon of the pair in a quantum buffer made of different fiber lengths as shown in Fig.2b. We use a counter-propagating scheme (CPS) [39, 40] to generate two-photon polarization entangled state $|\psi_o\rangle$ through a four-wave mixing process in a 300 m of dispersion-shifted fiber. The detailed experimental setup is shown in Fig.1S in the Supplementary. The signal and idler photons are separated by the DWDMs (dense wavelength-division multiplexing). The signal photon is sent to the polarization analyzer PA_s. The idler is sent to the buffer which consists of two low-loss switches and a single mode optical fiber as shown in Fig.2b. We can select the idler to pass a long or short fiber length.

When the idler is selected to pass the long fiber, then the idler is buffered with the duration of $\frac{L}{c/n_r}$, where L is the length of the fiber, and n_r is the refractive index of the fiber. The idler is then directed to the polarization analyzer PA_i . The first pair of the quarter-wave plate (QWP) and half-wave plate (HWP) is used to compensate for the birefringence of the fiber. The second pair of QWP and HWP is used to implement quantum state tomography. The timing of detecting the buffered photon can cause non-Markovian effect on the photon state [22, 41]. In this buffer configuration, the qubit storing process is initialized by two units of 1×2 switch. This switching process can impose loss and decoherence such as the amplitude/phase damping process. We use two units of 1×2 switch instead of one unit of 2×2 switch because the insertion loss of 1×2 switch (2×2 switch) is about < 0.01 dB (1.2 dB), respectively. To avoid decoherence due to timing issues on the photon detection, we operate the switch with low speed i.e. 1.0 Hz. In other words, we diminish the non-Markovian effect which can be caused by the switching process. We use an interface program to turn on and off the two switches synchronously at the rate of 1.0 Hz. The data is taken on the duration when both switches are completely turned on/off. We then perform quantum state tomography (QST) by using two single photon detectors (NuCrypt CPDS-4) operated at 50 MHz.

We characterize the prepared state $|\psi_o\rangle = (|H_s H_i\rangle + |V_s V_i\rangle)/\sqrt{2}$ by using the standard method of QST [42–44]. There are a total of 16 settings for the HWPs and QWPs in the PA_s and PA_i . For each setting, we measure the coincidence counts (CC) and accidentals (AC) with an integration time of 2 seconds or 100M sampling gates when the switches are turned on. Using the maximum likelihood estimation, we reconstruct the 4×4 density matrix of the final state ρ^f in the HV basis. We construct the density matrix ρ^f based on the true coincidence counts i.e. the accidental coincidence is subtracted. In other words, the Raman photon and loss-induced accidental do not contribute to this study. We repeat the state tomography for different fiber lengths from 0.0 m up to 25 km. The 0.0 m fiber length corresponds to the short path in the buffer.

We use the quantum discord to characterize the non-Markovian dynamics of the buffered photon. It is of both fundamental and practical interest to differentiate classical and quantum correlations within the total correlation for the buffered photon experiencing a non-Markovian environment. Two scenarios can contribute to the classical information; (1) environment projects or makes a measurement on the idler qubit state and creates the clas-

sical state, (2) environment perturbation can dechore the information of the idler qubit state such as degradation of the polarization properties. Scenario (1) is the classical correlation which will appear at the coincidence and accidental coincidence. We can avoid this classical correlation by subtracting the accidental. Scenario (2) can create a mixture of product states. We study the quantum discord under scenario (2) which can allow us to have a buffer time > 0.9 ms. For this purpose, we can accurately treat the final state as the Werner state. The Werner state is the mixture of the maximally entangled state with the probability P and the maximally mixed state as given by [44, 45],

$$\mathcal{W} = P|\psi_{\circ}\rangle\langle\psi_{\circ}| + \frac{1-P}{4}I. \quad (5)$$

where the I is the identity matrix. We calculate the average of the probability $P = \sum_i^{n=6} p'_i/n$, where $p'_{1(2)} = 4\rho'_{11(44)} - 1$, $p'_{3(4)} = 2\rho'_{14(41)}$, and $p'_{5(6)} = 1 - 4\rho'_{22(33)}$. The density matrix elements ρ'_{11} , ρ'_{44} , ρ'_{14} , ρ'_{41} , ρ'_{22} , and ρ'_{33} are obtained from the final state. The measured average probability P is the non-Markovian probability function $p(t)$. (See Method for Amplitude damping on one photon of two-photon Werner state). We plot the average probability P of the Werner state as a function of buffer time t as shown (red solid circle) in Fig.3. We fit the experiment data with the approximated probability function $\tilde{\mathcal{P}}_{a,sy} \propto e^{-A't}[1 - \mathcal{B}t^{\frac{1}{2}} + \mathcal{B}'t]$ as shown (red line) in Fig.3. This fitting formula is obtained from the combination of the approximated form of Eq. (3) and Eq. (4) with the substitution of $A' = 2\mu\frac{c}{n_r}$ and $L = (c/n_r)t$. The good fit of $\tilde{\mathcal{P}}_{a,sy}$ implies that the probability P of the Werner state exhibits non-Markovian dynamic. We obtain the fitting parameters A' , \mathcal{B} , and \mathcal{B}' . We then independently plot the exponential function $e^{-A't}$ (black line) and the harmonic functions (green line) of Eq. (3) and Eq. (4) in Fig.3. The parameter A' exhibits the exponential decay of the probability P where the loss parameter μ is the only dominant effect. The exponential feature can be observed at the buffer time (length) from 0 s (0 m) to 15 μ s (3.0 km). The parameters \mathcal{B} and \mathcal{B}' in the harmonic functions of Eq. (3) and Eq. (4) exhibit the PMD effect at the buffer time from 0s to 0.12 ms. We also fit the experiment data with the exact equations of Eq. (3) and Eq. (4). The exact equation exhibits a small oscillation within the error bar of the data as shown (blue line) in Fig.3. The exact equation of $\mathcal{P}_{a,sy}$ indicates a stronger non-Markovian dynamics than the approximated function of $\tilde{\mathcal{P}}_{a,sy}$. We further prove the existence of Markovian process if the idler photon is not buffered. We replace the buffer in the idler channel with a free-space attenuator and adjust the attenu-

ation α such that it equals to propagation loss (0.2 dB/km) \times the fiber length. We then perform the quantum state tomography on the signal and idler. We plot the probability P of the free-space attenuated entangled state (blue data point) as shown in Fig.3. We also fit the data with any arbitrary exponential function as shown (blue dotted line) in Fig.3. This indicates that the idler in free-space configuration is experiencing the Markovian dynamic without the fiber buffer i.e. without the coupling to the fiber birefringence and the fiber reservoir.

Since the approximated probability function $\tilde{\mathcal{P}}_{a,sy}$ and the exact equation $\mathcal{P}_{a,sy}$ fit well with the measured probability P of the Werner state, we can use the $\tilde{\mathcal{P}}_{a,sy}$ and the $\mathcal{P}_{a,sy}$ in quantum mutual information to quantify the quantum and classical correlation of the buffered photon and its paired photon. For a bipartite system, the total correlation, which is a measure of quantum mutual information, is given by $\mathcal{I}(\rho^f) = \mathcal{C}(\rho^f) + \mathcal{Q}(\rho^f)$, where the $\mathcal{C}(\rho^f)$ is classical correlation and the $\mathcal{Q}(\rho^f)$ is quantum discord. For the Werner state, the quantum discord is given by,

$$\mathcal{Q}(\rho^f) = \mathcal{I}(\rho^f) - \mathcal{C}(\rho^f) \quad (6)$$

where the total correlation and the classical correlation are given by [46, 47],

$$\begin{aligned} \mathcal{I}(\rho^f) &= \frac{3(1-P)}{4} \log_2(1-P) + \frac{(1+3P)}{4} \log_2(1+3P) \\ \mathcal{C}(\rho^f) &= \frac{(1-P)}{2} \log_2(1-P) + \frac{(1+P)}{2} \log_2(1+P) \end{aligned} \quad (7)$$

We also obtain the concurrence $\mathcal{C}_n(\rho^f) = \max\{0, \frac{(3P-1)}{2}\}$ for the Werner state in the system. We plot the quantum discord $\mathcal{Q}(\rho^f)$, classical correlation $\mathcal{C}(\rho^f)$, and concurrence \mathcal{C}_n as a function of the buffer time as shown in Fig.4. The experimental data is calculated based on the Eq. (6) where the probability P is obtained from the measured density matrix of the Werner state. We also calculate the quantum discord, classical, and concurrence by using the $P = \tilde{\mathcal{P}}_{a,sy}$ (solid line) and the $\mathcal{P}_{a,sy}$ (dotted line) which are obtained from the fitting curve of the approximated function and the exact equation of the Eq. (3) and Eq. (4), respectively, as shown in Fig.4. See Fig.S3 in the Supplementary for the extrapolation plot of the $\mathcal{I}(\rho^f)$, $\mathcal{C}(\rho^f)$, $\mathcal{Q}(\rho^f)$ and concurrence \mathcal{C}_n as a function of the buffer time up to 1.5 ms. When $P > \frac{1}{3}$ which is the well-known Werner's criterion for inseparable, the concurrent is not zero, so the Werner state is still entangled or inseparable[48]. When the $P = \frac{1}{3}$, the concurrent is 0. This occurs at the buffer time = 0.9 ms (190 km) which is numerically obtained from the fitting

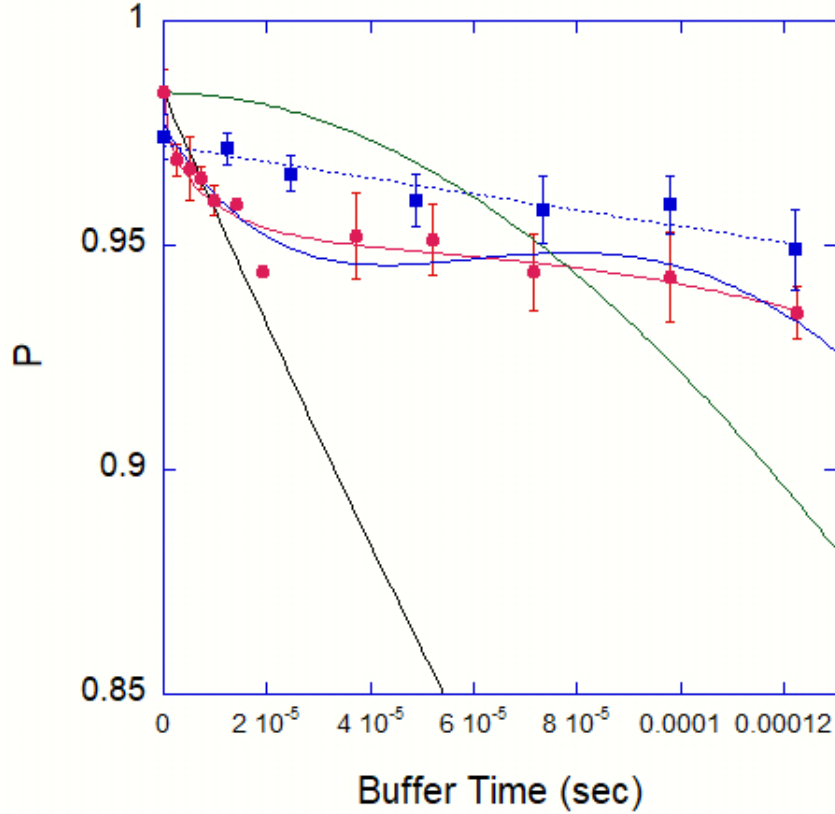


FIG. 3: The measured probability P of the Werner state as a function of buffer time for the buffer experiment (red solid circle) and the free-space attenuator (blue solid square). We convert the amount of the free-space attenuation ($\times 1/(0.2\text{dB/km})$) to buffer length and then to buffer time. Blue line (red solid line) is the fitting curve of the exact equation $\mathcal{P}_{a, sy}$ (the approximated function $\tilde{\mathcal{P}}_{a, sy}$) of Eq. (3) and Eq. (4), respectively. Blue dotted line is the fitting curve of an exponential function for the free-space attenuation. The plot of $e^{-A't}$ (black line). The plot of the harmonic functions of Eq. (3) and Eq. (4) (green line) $(\frac{\cos(Bt) - \sin(Bt)}{2})^2 + \cos(B't)^2$).

curve of the approximated function $\tilde{\mathcal{P}}_{a, sy} = \frac{1}{3}$ (see Fig.S2(a) in the Supplementary). As for the exact equation $\mathcal{P}_{a, sy} = \frac{1}{3}$, this falls at the buffer time = 0.4 ms (80 km) (see Fig.S2(b) in the Supplementary). The strength of the non-Markovian effect can determine the buffer time (fiber length) where the buffered photon can still preserve quantum entanglement. Since the

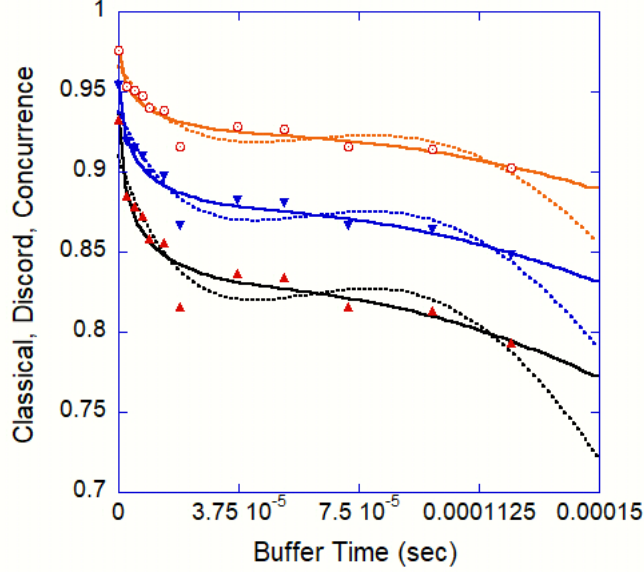


FIG. 4: The quantum discord \mathcal{Q} (blue line and blue dotted line), classical \mathcal{C} (black line and black dotted line), and concurrence \mathcal{C}_n (orange line and orange dotted line) of the Werner state as a function of buffer time by using the approximated probability function $\tilde{\mathcal{P}}_{a, sy}$ and the exact equation $\mathcal{P}_{a, sy}$, respectively. The experiment data: quantum discord (blue triangle), classical (red triangle), and concurrence (orange circle).

approximated function $\tilde{\mathcal{P}}_{a, sy}$ is a better fit, our data indicates that the fiber-based quantum buffer can preserve quantum entanglement with a buffer time of up to 0.9 ms.

Another interesting feature portrayed by the Werner state is the relationship between its concurrence, quantum discord and classical correlation. For the approximated function $0.523 < \tilde{\mathcal{P}}_{a, sy} < 1$, the concurrence is larger than the quantum discord and classical correlation in the range of the buffer time (length) from 0 s(0 m) to 0.7 ms(145 km). The $\tilde{\mathcal{P}}_{a, sy} = 0.532$ occurs at the buffer time = 0.7 ms as shown in Fig.S2(a) in the Supplementary. Similarly, for the exact equation $\mathcal{P}_{a, sy} = 0.532$, this falls at the buffer time = 0.3 ms (64 km) as shown in Fig.S2(b) in the Supplementary. The most important feature of the quantum mutual information is the quantum discord $\mathcal{Q}(\rho^f) >$ the concurrence and the classical correlation. This occurs at the buffer time larger than 0.7 ms(0.3 ms) in the approximated function $\tilde{\mathcal{P}}_{a, sy}$ (exact equation $\mathcal{P}_{a, sy}$), respectively.

DISCUSSION

To our knowledge, this measurement is the first demonstration based on a simple qubit-fiber birefringence-reservoir model to study the non-Markovian effect on a two-photon polarization entangled state in which one photon from the pair is stored in a buffer made of different fiber lengths. We subtract the accidental coincidence in our data analysis so that the loss parameter μ is mainly contributed from the degradation of the polarization extinction ratio of the photonic qubit. One can regard the μ as the strength of the environment depolarization effect on the buffered photon. Our finding indicates that the density matrix $\rho(t)$ of the entangled state at the output of the buffer is related to its early $\rho(t')$ in the buffer, where $t > t'$. This occurs when the environment depolarization effect of the fiber is more dominant than the PMD effect. We also demonstrate the Markovian scenario where the PMD effect did not exist by replacing the buffer with a free-space attenuator representing a memory-less environment.

We use the Werner state as the final state for the buffered idler photon and its paired signal photon. The Werner state is entangled (inseparable) when the $P > \frac{1}{3}$. The concurrence is zero at $P = \frac{1}{3}$ which is the Werner's well known separability criterion. The entanglement is related to the concurrence as $E_n(\rho_{AB}) = H((1 + \sqrt{1 - \mathcal{C}_n^2})/2)$, where the \mathcal{C}_n is the concurrence, and the function $H(x) = -x \log_2 x - (1 - x) \log_2(1 - x)$ is the Shannon entropy. When the concurrence is zero, the entanglement is also zero at $P = \frac{1}{3}$. Based on this criterion, we can design the optimum fiber length of up to 190 km for the buffer in which the state is still inseparable or entangled. This buffer length corresponds to the buffer time of 0.9 ms.

Several measures of detecting the non-Markovian dynamics have been proposed[49, 50]. Our approach here of using quantum state tomography to find the probability function $p(t)$ leads us to the measures of quantum mutual information such as classical correlation and quantum discord. We then use the quantum discord to characterize the quantum correlation of the entangled state in our buffer system. Quantum discord is a better concept than entanglement to characterize the quantum correlation of a quantum system [48]. The quantum discord is nonzero at $P = \frac{1}{3}$ where the concurrence is zero. (see Fig.S2 in the Supplementary). The non-zero quantum discord can surpass Werner's criterion on the optimum buffer time. The quantum discord implies that the quantum bi-partite correlation still exists for

buffer time greater than 0.9 ms.

The possibility for the buffered photon to experience the case $\Delta\phi_h \neq \Delta\phi_v$ (see the detail in Method: the probability function for $\Delta\phi_h \neq \Delta\phi_v$) is rare for the single-mode fiber which is used for communication network. The reason is that the distributed fiber has a homogenous refractive index. The PMD effect of a light field in the single-mode fiber should not depend on the input polarization state of the light. However, the case $\Delta\phi_h \neq \Delta\phi_v$ may occur for the photon buffered in a loop of fiber more than one round trip. We are currently investigating the quantum buffer made of a fiber loop in a 2x2 Switch configuration[51], where the photon is buffered by passing the same fiber loop multiple times.

Our analytical approach to derive the probability function can be easily extended to two qubits interacting separately with two independent non-Markovian environments such as the idler and the signal are buffered independently in two different buffers. It has been demonstrated that the non-Markovian density matrix evolution on one qubit state can be mathematically proceeded to the density matrix of two-qubit entangled state [27–29, 52]. The strength of the non-Markovian effect will be proportional to the square of Eq. (3) and Eq. (4), and hence will reduce the optimum buffer time. However, one can design the parameters κ and γ_o so that the crossover between Markovian and non-Markovian on the qubits can be controlled and utilized for modeling quantum networks [22, 23]. We may improve the fiber-based quantum buffer by using the ultra-low loss single mode fiber such as SMF-28-ULL (Corning) and low loss Z-fiber from Sumitomo Electric, so that we can control the buffer to exhibit the Markovian effect, where its $\rho(t)$ is not related to $\rho(t')$ in the buffer.

METHODS

Atom-Cavity-Reservoir Model. Our analytical approach is similar to a qubit of a two-level atom interacting in a high Q-cavity, which is coupled to the reservoir with the Lorentzian spectral distribution [30, 31]. The cavity-reservoir coupling gives rise to the effective spectral density in the form of, $(\gamma_o\Lambda^2)/[(\omega_o - \omega)^2 + \Lambda^2]$, where the parameter γ_o is the coupling constant between the cavity and the reservoir. The parameter Λ is the spectral width of the reservoir. The atom transition frequency and the cavity are in resonance with $\omega_o = \omega_{\text{cavity}}$. When the Λ becomes very large or approaches infinity, the reservoir is considered memoryless or Markovian. Then, the cavity is only the main cause of the

non-Markovian dynamic in the system. The diagonal (off-diagonal) density matrix elements of atomic qubit are evolving in time t as a function of $p(t) \propto e^{-\frac{\gamma_o t}{2}} [\cos(\frac{\delta t}{4}) + \frac{\gamma_o}{\delta} \sin(\frac{\delta t}{4})]^2$ ($\sqrt{p(t)}$), respectively, where $\delta = \sqrt{16\kappa^2 - \gamma_o^2}$, and κ is the coupling constant between the atomic qubit and the cavity and related to the decay rate of the excited state. The parameter δ can be used to determine whether the system is Markovian ($4\kappa < \gamma_o$) or non-Markovian ($4\kappa \geq \gamma_o$).

The relationship of γ_o and κ on the Markovian and non-Markovian processes.

The density matrix of the photon state is dependant on the probability function [30, 31] $p(t) \propto e^{-\frac{\gamma_o t}{2}} [\cos(\frac{\delta t}{4}) + \frac{\gamma_o}{\delta} \sin(\frac{\delta t}{4})]^2$, where t is the propagation time of the photon in the fiber. The parameter $\delta = \sqrt{16\kappa^2 - \gamma_o^2}$ can be used to determine whether our open quantum system is Markovian or non-Markovian.

For $4\kappa < \gamma_o$ or $1 < \frac{\gamma_o}{4\kappa}$, $\delta \rightarrow i\delta$, the harmonic function $\sin(\cdot)$ and $\cos(\cdot)$ becomes hyperbolic function $\cosh(\cdot)$ and $\sinh(\cdot)$, respectively. Our quantum system is undergoing Markovian dynamics. This occurs when the PMD and the loss parameter are the dominant effects on the photonic qubit. Hence, the probability function $p(t)$ becomes an exponential function. The polarization mode dispersion (PMD) effect that leads to the Markovian process i.e. entanglement sudden death has been experimentally observed [53] and theoretically studied [54] on the fiber-based entangled photon pair. One can enhance the PMD effect on photon pairs by increasing their differential group delays such as inserting a few polarization-maintaining fiber jumpers in their channels.

For $4\kappa \geq \gamma_o$, where the PMD effect is less dominant than the loss parameter, our system becomes non-Markovian. For simplicity, we assume $\gamma_o = 4\kappa/n$ where $n > 1$, then $\delta \sim 4\kappa$. Then, the harmonic function of $p(t)$ depends only on the PMD effect. In general, our system is subjected to non-Markovian dynamics and then the probability function of the qubit is given by,

$$p(t) \propto e^{-\frac{\gamma_o}{2}t} [\cos(\kappa t) + \frac{1}{n} \sin(\kappa t)]^2. \quad (8)$$

However, our analytical approach can provide a new physical insight into the coupling constant (κ) of the PMD and the loss (μ) effects on the two-photon polarization entangled state when one photon from the pair is stored in a fiber-based quantum buffer.

Amplitude Damping on one photon from the two-photon Werner State. The

amplitude damping process on one qubit from two-qubit Werner state ρ is given by,

$$\rho' = E_o \rho E_o^\dagger + E_1 \rho E_1^\dagger = \begin{pmatrix} \frac{1-p}{4} & 0 & 0 & \frac{p\sqrt{1-\xi}}{2} \\ 0 & \frac{(1-p)(1-\xi)}{4} + \frac{(1+p)(\xi)}{4} & 0 & 0 \\ 0 & 0 & \frac{1-p}{4} & 0 \\ \frac{p\sqrt{1-\xi}}{2} & 0 & 0 & \frac{(1+p)(1-\xi)}{4} + \frac{(1-p)(\xi)}{4} \end{pmatrix}$$

where $E_o = (I \otimes \Gamma_o)$ and $E_1 = (I \otimes \Gamma_1)$. The identity matrix $I = \begin{pmatrix} 1 & 0 \\ 0 & 1 \end{pmatrix}$. The

amplitude damping operators are $E_o = \begin{pmatrix} 1 & 0 \\ 0 & \sqrt{1-\xi} \end{pmatrix}$ and $E_1 = \begin{pmatrix} 0 & \sqrt{\xi} \\ 0 & 0 \end{pmatrix}$, where the ξ is the probability of depolarizing a photon. We measure the density matrix ρ' and obtain the density matrix elements $\rho'_{11} = \frac{1+p'_{11}}{4}$, $\rho'_{22} = \frac{1-p'_{22}}{4}$, $\rho'_{33} = \frac{1-p'_{33}}{4}$, $\rho'_{44} = \frac{1+p'_{44}}{4}$, $\rho'_{14} = \frac{p'_{14}}{2}$, and $\rho'_{41} = \frac{p'_{41}}{2}$. From each density matrix elements, we write $p'_{nm(n,m=1,2,3,4)}$ in term of p of the Werner State ρ such as;

$$p'_{11} = p'_{33} = p \quad (9)$$

$$p'_{22} = p'_{44} = p(1 - 2\xi) \quad (10)$$

$$p'_{14} = p'_{41} = p\sqrt{1-\xi} \simeq p(1-\xi). \quad (11)$$

where we approximate $p\sqrt{1-\xi} \simeq p(1-\xi)$ for $\xi < 0.04(4\%)$. Our experimental data indicates that p drops less than 4%. We then take the average of the measured $\frac{p'_{11}+p'_{22}+p'_{33}+p'_{44}+p'_{14}+p'_{41}}{6} = \frac{6p-5p\xi}{6} \sim p(1-\xi) = p(t)$. The $p(t)$ is the non-Markovian probability function. It shows that the p of the Werner state is changing by $(1-\xi)$.

The probability function for $\Delta\phi_h \neq \Delta\phi_v$. For the situation $\Delta\phi_h \neq \Delta\phi_v$, Eq. (2) can be rewritten as

$$\begin{aligned} \mathcal{P}_\pm^f &= e^{-2\mu L} [2 + 2 \cos(\Delta\phi_v) \cos(\Delta\phi_h) \\ &\quad - 2 \sin(\pm\Delta\phi_h) \sin(\pm\Delta\phi_v) - 2 \cos(\Delta\phi_h) \sin(\pm\Delta\phi_v) \\ &\quad + 2 \cos(\Delta\phi_h) \sin(\pm\Delta\phi_h) - 2 \cos(\Delta\phi_v) \sin(\pm\Delta\phi_v) \\ &\quad + 2 \cos(\Delta\phi_v) \sin(\pm\Delta\phi_h)]. \end{aligned} \quad (12)$$

To simplify the above expression, we assume $\Delta\phi_{h(v)}$ is relatively small and substitute $\cos(\Delta\phi) = 1 - \frac{\Delta\phi^2}{2}$ and $\sin(\Delta\phi) = \Delta\phi$ to the \mathcal{P}_\pm^f . The first few terms of the \mathcal{P}_\pm^f are given as;

$$\mathcal{P}_{\pm}^f \propto e^{-2\mu L} [2 + \pm \mathcal{B}L^{\frac{1}{2}} \pm \mathcal{B}'L \mp \mathcal{C}L^{\frac{3}{2}} \pm \mathcal{C}'L^2 \pm \mathcal{C}L^{\frac{5}{2}} \pm ..]. \quad (13)$$

This approximated probability function is depending on the power of the fiber length $L^{\frac{n}{2}}$, where the n is positive integer number.

DATA AVAILABILITY

The data that supports the findings of this study are available from the corresponding author upon reasonable request.

* `kim.lee@northwestern.edu`

REFERENCES

- [1] Sangouard, Nicolas, Simon, Christoph, de Riedmatten, H. & Gisin, N. Quantum repeaters based on atomic ensembles and linear optics. *Rev. Mod. Phys.* **83**, 33-80 (2011).
- [2] Dou, J.P., Yang, A.L., Du, M.Y. et al. A broadband DLCZ quantum memory in room-temperature atoms. *Commun Phys* **1**, 55 (2018).
- [3] Wang, Y., Li, J., Zhang, S., Su, K., Zhou, Y., Liao, K., Du, S., Han, Y. & Zhu, S.L. Efficient quantum memory for single-photon polarization qubits. *Nat. Photon.* **13**, 346-351 (2019).
- [4] Lvovsky, A., Sanders, B. & Tittel, W. Optical quantum memory. *Nat. Photon.* **3**, 706-714 (2009).
- [5] Holzzapfel, A., Etesse, J., Kaczmarek, K. T., Tiranov, A., Gisin, N. & Afzelius, M. Optical storage for 0.53 seconds in a solid-state atomic frequency comb memory using dynamical decoupling. *New J. Phys.* **22**, 063009 (2020).
- [6] Li, Xi., Voss, P. L., Chen, J., Sharping, J. E. & Kumar, P. Storage and long-distance distribution of telecommunications-band polarization entanglement generated in an optical fiber. *Opt. Lett.* **30**, 1201-1203 (2005).
- [7] Arnold, N. T., Victora, M., Goggin, M. E. & Kwiat, P. G. All-optical ultrawide-bandwidth quantum buffer. *Proc. SPIE, Photonics for Quantum* **11844**, 118440Y (2021).

- [8] Kaneda, F., Xu, F., Joseph, C. & Kwiat, P. G. Quantum-memory-assisted multi-photon generation for efficient quantum information processing. *Optica* **4**, 1034-1037 (2017).
- [9] Wang, X. & Mookherjea, S. Feasibility of chipscale integration of single-photon switched digital loop buffer. *Chip* **1**, 100028 (2022). <https://doi.org/10.1016/j.chip.2022.100028>
- [10] Takesue, H., Matsuda, N., Kuramochi, E. et al. An on-chip coupled resonator optical waveguide single-photon buffer. *Nat. Commun.* **4**, 2725 (2013).
- [11] Eunjoon Lee, Sang Min Lee & Hee Su Park. Relative time multiplexing of heralded telecom-band single-photon sources using switchable optical fiber delays. *Opt. Express* **27**, 24545-24555 (2019).
- [12] S. Clemmen, Alessandro Farsi, Sven Ramelow & Alexander L. Gaeta. All-optically tunable buffer for single photons. *Opt. Lett.* **43**, 2138-2141 (2018).
- [13] G. J. Mendoza, R. Santagati, J. Munns, E. Hemsley, M. Piekarek, E. Martin-Lopez, Graham D. Marshall, Damien Bonneau, Mark G. Thompson & Jeremy L. O'Brien. Active temporal and spatial multiplexing of photons. *Optica* **3**, 127-132 (2016).
- [14] Lee, K. F., Moraw, P. M., Reilly, D. R. & Kanter, G. S. Pulse Retiming for Improved Switching Rates in Low-Noise Cross-Phase-Modulation-Based Fiber Switches. *IEEE Photonics Technology Letters* **33**, 51-54 (2021) doi: 10.1109/LPT.2020.3044256.
- [15] Lee, K. F. & Kanter, G. S. Low-Loss High-Speed C-Band Fiber-Optic Switch Suitable for Quantum Signals. *IEEE Photonics Technology Letters* **31**, 705-708 (2019) doi: 10.1109/LPT.2019.2905593
- [16] Zhong, W. D. & Tucker, R. S. A new wavelength-routed photonic packet buffer combining traveling delay lines with delay-line loops. *J. Lightwave Technol.* **19**, 1085-1092 (2001).
- [17] Langenhorst, R., Eiselt, M., Pieper, W., Grosskopf, G., Ludwig, R., Kuller, L., Dietrich, E. & H. G. Weber. Fiber loop optical buffer, *J. Lightwave Technol.* **14**, 324-335 (1996).
- [18] Kaneda, F., Christensen, B. G., Wong, J. J., Park, H. S., McCusker, K. T & Kwiat, P. G. Time-multiplexed heralded single-photon source. *Optica* **2**, 1010 (2015).
- [19] C. Xiong, C., Zhang, X., Liu, Z., Collins, M. J., Mahendra, A., Helt, L. G., Steel, M. J., Choi, D. Y., Chae, C. J., Leong, P. H. W. & Eggleton, B. J. Active temporal multiplexing of indistinguishable heralded single photons. *Nat. Commun.* **7**, 10853 (2016).
- [20] Mele Francesco Anna, Lami Ludovico & Giovannetti, Vittorio. Restoring Quantum Communication Efficiency over High Loss Optical Fibers. *Phys. Rev. Lett.* **129**, 180501 (2022).

- [21] Giovannetti, V. A dynamical model for quantum memory channels. *J. Phys. A: Math. Gen.* **38**, 10989 (2005).
- [22] Helsen, J. & Wehner, S. A benchmarking procedure for quantum networks. *npj Quantum Inf* **9**, 17 (2023).
- [23] Rivas, A., Huelga, S. F. & Plenio, M. B. Quantum non- markovianity: characterization, quantification and detection. *Rep. Prog. Phys.* **77**, 094001 (2014).
- [24] Liu, B.H., Li, L., Huang, Y.F. et al. Experimental control of the transition from Markovian to non-Markovian dynamics of open quantum systems. *Nature Phys.* **7**, 931-934 (2011). <https://doi.org/10.1038/nphys2085>
- [25] Haase, J. F. et al. Controllable non-markovianity for a spin qubit in diamond. *Phys. Rev. Lett.* **121**, 060401 (2018).
- [26] Wang, F. et al. Observation of entanglement sudden death and rebirth by controlling a solid-state spin bath. *Phys. Rev. B* **98**, 064306 (2018).
- [27] Breuer, H.P. & Petruccione, F. Theory of OpenQuantum Systems. *Oxford University Press, Oxford, New York* (2002).
- [28] Maniscalco, S. & Petruccione, F. Non-Markovian dynamics of a qubit. *Phys. Rev. A.* **73**, 012111 (2006).
- [29] Bellomo, B., Lo Franco, R. & Compagno, G. Non-Markovian Effects on the Dynamics of Entanglement. *Phys. Rev. Lett.* **99**, 160502 (2007).
- [30] Ma, Tiantian, Chen, Yusui, Chen, Tian, Hedemann, Samuel R. & Yu, T. Crossover between non-Markovian and Markovian dynamics induced by a hierarchical environment. *Phys. Rev. A.* **90**, 042108 (2014).
- [31] Wang, D., Huang, A.J., Hoehn, R.D. et al. Entropic uncertainty relations for Markovian and non-Markovian processes under a structured bosonic reservoir. *Sci. Rep.* **7**, 1066 (2017). <https://doi.org/10.1038/s41598-017-01094-8>
- [32] Wang Bo, Xu Zhen-Yu, Chen Ze-Qian & Feng, M. Non-Markovian effect on the quantum discord. *Phys. Rev. A* **81**, 014101 (2010)
- [33] Fanchini, F. F. and Werlang, T. and Brasil, C. A. & Arruda, L. G. E. and Caldeira, A. O. Non-Markovian dynamics of quantum discord. *Phys. Rev. A* **81**, 052107 (2010).
- [34] Shi, S., Kumar, P & Lee, K.F. Generation of photonic entanglement in green fluorescent proteins. *Nat. Commun* **8**, 1934 (2017).

- [35] Shi, S. et al. Broadband photon pair generation in green fluorescent proteins through spontaneous four-wave mixing. *Sci. Rep.* **6**, 24344; doi: 10.1038/srep24344 (2016).
- [36] Kogelnik, H., Jopson, R. M. & Nelson, L. E. Polarization-Mode Dispersion. *Optical Fiber Telecommunications 4A*, I. P. Kaminow and T. Li, Eds. (Academic Press, Boston) Chap.15 (2002).
- [37] Wai, K. A. & Menyuk, C. R. Polarization Mode Dispersion, Decorrelation, and Diffusion in Optical Fibers with Randomly Varying Birefringence. *J. Lightwave Technol.* **14**, 148 (1996).
Brodsky Lightwave Journal
- [38] Brodsky, M., Frigo, N. J., Boroditsky, M. & Tur, M. Polarization Mode Dispersion of Installed Fibers. *J. Lightwave Technol.* **24**, 4584-4599 (2006).
- [39] Lee, K. F., Chen, J., Liang, C. , Li, X., Voss, P. L. & Kumar, P. Generation of high-purity telecom-band entangled photon pairs in dispersion-shifted fiber. *Opt. Lett.* **31**, 1905-1907 (2006).
- [40] Sua, Y. M., Malowicki, J. & Lee, K. F. Quantum correlation of fiber-based telecom-band photon pairs through standard loss and random media. *Opt. Lett.* **39**, 4808-4811 (2014).
- [41] Humphreys, P. C. et al. Deterministic delivery of remote entanglement on a quantum network. *Nature* **558**, 268-273 (2018).
- [42] James, Daniel F. V., Kwiat, Paul G., Munro, W. J. & White, A. G. Measurement of qubits. *Phys. Rev. A.* **64**, 052312 (2001).
- [43] White, A. G., James, D. F., Munro, W. J. & Kwiat, P. G. Exploring Hilbert space: Accurate characterization of quantum information. *Phys. Rev. A.* **65**, 012301 (2001).
- [44] Munro, W. J., James, D. F., White, A. G. & Kwiat, P. G. Maximizing the entanglement of two mixed qubits. *Phys. Rev. A.* **64**, 030302 (2001).
- [45] R. F. Werner. Quantum states with Einstein-Podolsky-Rosen correlations admitting a hidden-variable model. *Phys. Rev. A* **40**, 4277 (1989).
- [46] Luo, S. Quantum discord for two-qubit systems. *Phys. Rev. A* **4**, 042303 (2008).
- [47] Ali, Mazhar, Rau, A. R. P. & Alber, G. Quantum discord for two-qubit X states *Phys. Rev.* **81**, 042105 (2010).
- [48] Ollivier, H. & Zurek, W. H. Quantum Discord: A Measure of the Quantumness of Correlations. *Phys. Rev. Lett.* **88**, 017901 (2001).
- [49]

- [50] Rivas, A., Huelga, S. F. & Plenio, M. B. Entanglement and Non-Markovianity of Quantum Evolutions. *Phys. Rev. Lett.* **105**, 050403 (2010).
- [51] Kim Fook Lee, Gamze Gul, Zhao Jim & Prem Kumar. Fiber Loop Quantum Buffer for Photonic Qubits. <https://doi.org/10.48550/arXiv.2309.07987>
- [52] Bellomo, B., Lo Franco, R. & Compagno, G. Entanglement dynamics of two independent qubits in environments with and without memory. *Phys. Rev. A* **77**, 032342 (2008).
- [53] Brodsky, M., George, E.C., Antonelli, C. & Shtaiif, M. Loss of polarization entanglement in a fiber-optic system with polarization mode dispersion in one optical path. *Opt. Lett.* **36**, 43-45 (2011).
- [54] Antonelli, C., Shtaiif, M. & Brodsky, M. Sudden Death of Entanglement Induced by Polarization Mode Dispersion. *Phys. Rev. Lett.* **106**, 080404 (2011).

ACKNOWLEDGMENTS

This work was supported in part by the DOE (DE-SC0020537)

AUTHOR CONTRIBUTIONS

K.F.L and P.K conceived the research. K.F.L analyzed the data, wrote the paper and prepared the manuscript.

COMPETING INTERESTS

The authors declare no competing interests.

Supplementary Document: Non-Markovian Dynamics in Fiber Delay-Line Buffers

Kim Fook Lee and Prem Kumar¹

¹*Center for Photonic Communication and Computing,
Department of Electrical Engineering and Computer Science,
Northwestern University, 2145 Sheridan Road, Evanston, IL 60208-3112, USA**

(Dated: Compiled February 2, 2024)

Abstract

This document provides supplementary materials for "Non-Markovian Dynamics in Fiber Delay-Line Buffers".

Supplementary Information

Contents:

1. Fig. S1 The counter-propagating scheme (CPS) with the 300 m dispersion shifted fiber.
2. Fig. S2 The extrapolation plot of total, classical , quantum discord, and concurrence as a function of probability.
3. Fig. S3 The extrapolation plot of total, classical , quantum discord and concurrence with the buffer time t up to 1.5 ms.

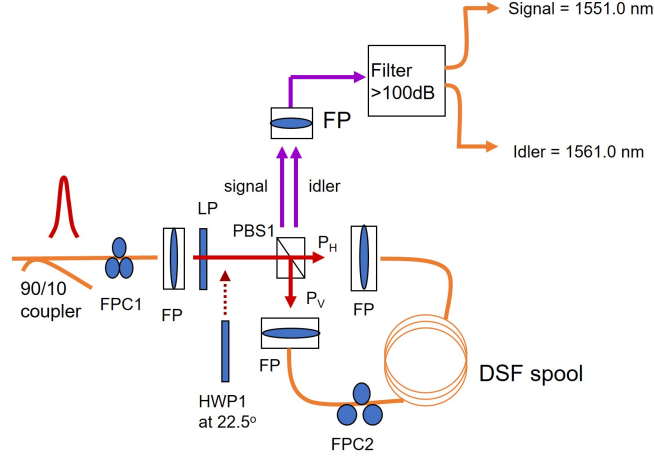


FIG. S1: The counter-propagating scheme (CPS) with the 300 m dispersion shifted fiber. The pump wavelength is at 1556 nm. The pump laser is operated at 50 MHz with the pulse duration of 5.0 ps. The half-wave plate (HWP1) before the polarizing beam splitter (PBS1) is used to prepare the pump to horizontally (P_H) and vertically (P_V) polarized pumps. The P_H (P_V) pumps generated signal and idler in the clockwise (counter-clockwise) direction through the spontaneous four-wave mixing process in a 300 m dispersion-shifted fiber. The two-photon polarization entangled state $|\psi_o\rangle = \frac{1}{\sqrt{2}}[|H_s H_i\rangle + |V_s V_i\rangle]$ is then created at the output of PBS1. FP: fiber port; FPC: fiber polarization controller.

* kim.lee@northwestern.edu

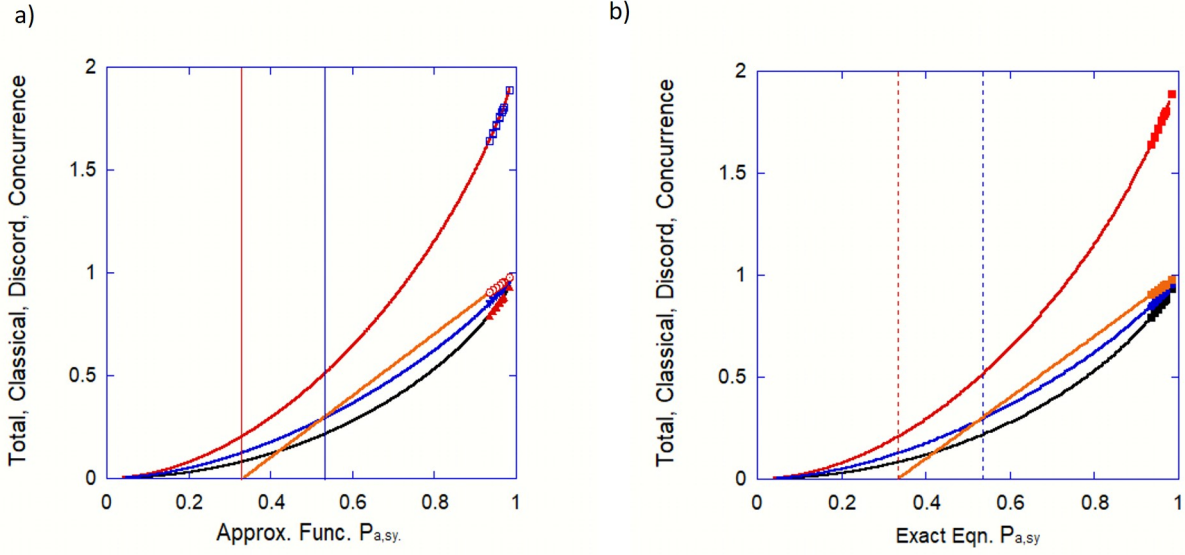


FIG. S2: (a) The extrapolation plot of total, classical, quantum discord, and concurrence as a function of probability $\tilde{\mathcal{P}}_{a, sy}$. The vertical red line marks the location when $\tilde{\mathcal{P}}_{a, sy} = 0.333$ occurs at buffer time (fiber length) = 0.9 ms (190 km). The vertical blue line marks the location when $\tilde{\mathcal{P}}_{a, sy} = 0.523$ occurs at buffer time (fiber length) = 0.7 ms (145 km). (b) As for the extrapolation plot with the exact equation of $\mathcal{P}_{a, sy}$, the vertical red dotted line marks the location when $\mathcal{P}_{a, sy} = 0.333$ occurs at buffer time (fiber length) = 0.4 ms (80 km). The vertical blue dotted line marks the location when $\mathcal{P}_{a, sy} = 0.523$ occurs at buffer time (fiber length) = 0.3 ms (64 km).

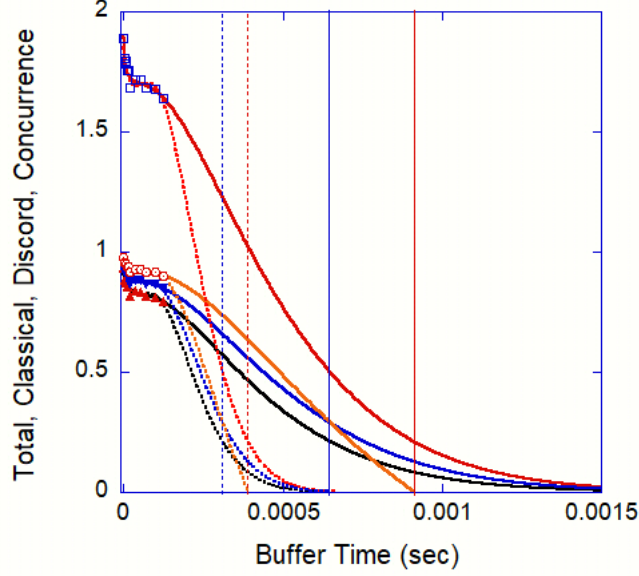


FIG. S3: The extrapolation plot of total, classical, quantum discord and concurrence with the buffer time t up to 1.5 ms. The total \mathcal{I} (red line), classical \mathcal{C} (black line), quantum discord \mathcal{Q} (blue line), and concurrence \mathcal{C}_n (orange line) of the Werner state as a function of buffer time. The experiment data: total (blue square), quantum discord (blue triangle), classical (red triangle), and concurrence (orange circle). The plot of the total (red dotted line), quantum discord (blue dotted line), classical (black dotted line), and concurrence (orange dotted line) by using the exact equation of $\mathcal{P}_{a, sy}$. The vertical red line marks the location when $\tilde{\mathcal{P}}_{a, sy} = 0.333$ occurs at buffer time (fiber length) = 0.9 ms (190 km). The vertical blue line marks the location when $\tilde{\mathcal{P}}_{a, sy} = 0.523$ occurs at buffer time (fiber length) = 0.7 ms (145 km). As for the extrapolation plot with the exact equation of $\mathcal{P}_{a, sy}$, the vertically dotted red line marks the location when $\mathcal{P}_{a, sy} = 0.333$ occurs at buffer time (fiber length) = 0.4 ms (80 km). The vertically dotted blue line marks the location when $\mathcal{P}_{a, sy} = 0.523$ occurs at buffer time (fiber length) = 0.3 ms (64 km).